e-ISSN: 2548-060X

International Journal of Energy Applications and Technologies

journal homepage: https://dergipark.org.tr/en/pub/ijeat

Original Research Article

Electromechanical modeling of energy harvesting for FRP composite structures coupled with piezoelectric transducers

Hakan Uçar*

Piri Reis University, Faculty of Engineering, Department of Mechanical Engineering, Istanbul, Türkiye

ARTICLE INFO

* Corresponding author
hucar@pirireis.edu.tr

Received December 7, 2021
Accepted March 31, 2022

Published by Editorial Board Members of IJEAT

doi: 10.31593/ijeat.1033539

ABSTRACT

Supplanting of metals by composites is on the rise for the last three decades in the aerospace, marine and automotive industry following the trend of electrification and indigenous design approaches. In parallel, piezoelectric (PZT) sensors and energy harvesters have gained significant attention due to their applicability and efficacy for microscale power generation systems. From a new perspective, embedding PZT sensors into composite structures will be beneficial in many aspects. Condition monitoring can be performed by using the sensing capability of PZTs while vibration can be controlled by means of its excitation capability. Besides, energy harvesting can be employed due to the mechanical forces exerted on the coupled structure. It is critical to create an accurate numerical modeling of electromechanical coupling for the investigation of efficiency of PZT sensors. In this paper, electromechanical modeling of a Fiber Reinforced Polymer (FRP) composite structure with an embedded PZT patch is presented and validated with an experimental setup. Afterwards, the energy harvesting capability of a PZT patch embedded in the FRP structure is investigated.

Keywords: Electromechanical modeling; Energy harvesting; Finite element method; FRP; Piezoelectric

1. Introduction

Lately, shortcomings in energy resources have made energy harvesting an important issue. Energy harvesting is basically the conversion of existing ambient energy into electrical energy. One of the most widely used materials for this purpose is piezoelectric material with its high power density, transduction capacity and functionality in high frequency applications [1]. Piezoelectric materials have the ability to convert mechanical energy into electrical energy as a result of mechanical deformation and vice versa. Thus, these materials are widely used as sensors [3, 4] and energy harvesters [5, 6]. On the other hand, by using the converse effect of the piezoelectric material, they can be used as actuators [7-9].

Piezoelectric energy harvesting is mainly applied for harvesting small-scale energy to be supplied for low power electronics [2]. In order to achieve a sufficient energy harvesting, the effectiveness of the PZT sensors must be well defined. For this reason, it is necessary to conduct energy harvesting experiments prior to the use on-site. However, these experiments pose significant costs and time consumption. Therefore, it has become crucial to conduct computer analysis with verified benchmarking studies for modeling the electromechanical coupling. Within this scope, analytical models such equivalent circuits [10], spring models [11] and thermal analogy [12] are applied for two-dimensional analysis. For three-dimensional analysis, Finite Element Method (FEM) is a convenient tool that provides detailed analysis of structures and predicts the behavior of electromechanical structures under real conditions at a lower cost and more quickly [13, 14]. Accordingly, many studies have been carried out on the application of FEM for electromechanical coupling modeling and piezoelectric energy harvesting. V. Nguyen et. al [15] presented the

development of a three-dimensional finite element (FE) model for characterizing the piezoelectric actuators. In other study, the use of shell elements for electromechanical FE analysis of composite and sandwich multilayered structures [16]. S. Avdiaj et. al [17] investigated the piezoelectric effect using FEM and showed that FE model is applicable for microstructures. Liao et al [18] proposed a new method which enables FE formulations to design and optimize piezoelectric energy harvesters and they validated the proposed method experimentally. In another study, an FE model was developed to predict the effects of the static pre-stress and coupling efficiency on the pre-stressed piezoelectric stack energy harvester [19]. Dash et. al [20] presented a novel FE model for characterization of the galloping based piezoelectric energy harvesters. Likewise, Song [21] investigated a piezoelectric energy harvester subjected to traffic-induced vibration of a railway bridge with an FE application and Chowdhury at. al [22] presented the effect of porous auxetic structure on low-frequency piezoelectric energy harvesting systems by conducting an FE study.

In this study, the electromechanical modeling is of an Aramid FRP (AFRP) composite beam coupled with a PZT patch is introduced. FE model of the beam is created and direct effect of the piezoelectricity is presented. Results are validated with the experimental results. Once the electromechanical modeling is validated, energy harvesting capabilities of PZT patch embedded in the AFRP beam are investigated numerically.

The paper is organized as follows. Section 2 presents the theory of electromechanical modeling of the beam highlighting the governing equations. In Section 3, the numerical model of AFRP beam with a PZT patch and validation is introduced and the energy harvesting capabilities are presented. Finally, Section 4 concludes the paper.

2. Theory of Electromechanical Modeling

For linear piezoelectricity, the interaction between stress, strain, electric charge and electric field is defined in the electromechanical constitutive equations [23], given as follows;

$$\sigma_{ij} = C^{E}_{ijkl}\,\varepsilon_{kl} - e_{ijk}\,E_k \tag{1}$$

$$D_i = e_{ikl}\,\varepsilon_{kl} + \epsilon^{S}_{ij}\,E_j \tag{2}$$

where σ_{ij} is the component of stress tensor; D_i is the component of electric displacement vector; ε_{kl} is the component of strain tensor; E is the electric field vector; C_{ijkl} is the elastic constant; ϵ_{ij} is the dielectric material constant and e_{ijk} is the piezoelectric constant. Subscripts $()_i$ and $()_{ij}$ represent the corresponding component of a vector and a matrix, respectively. Superscript E stands for constant electrical field while S represents constant strain, where the elastic stiffness and permittivity parameters are obtained.

According to the electromechanical coupling defined in Equation (2), the mechanical strain is transformed to electrical charge. This is referred as direct piezoelectric effect and allows piezoelectric materials to be used as sensors and energy harvesters. On the contrary, the electromechanical coupling described in Equation (1) enables the conversion of electrical energy into mechanical energy, by which allows piezoelectric materials to be used as actuators.

Equation of motion of the electromechanical system can be derived according to the Hamilton principle along with the virtual work theory for a virtual displacement field δu_i and the potential δV. Electric field, in Equation (1) and (2) is associated with the electrical potential V as in Equation (3).

$$E = -grad\,V \tag{3}$$

In a FEM analysis, the domain is divided into a finite number of small elements having geometrically simple shapes. The unknowns in electromechanical model such as mechanical displacement, u, exciting force, f, electrical potential, V and the charge, q are determined and stored at the nodes of these elements.

The displacement field, $\{u\}$ and the electric potential, $\{V\}$ can be determined by establishing nodal solutions and corresponding shape functions defined as in Equation (4) and (5).

$$\{u\} = [N_u]^T\{u_i\} \tag{4}$$

$$\{V\} = [N_V]^T\{V_i\} \tag{5}$$

where $\{u_i\}$, $\{V_i\}$, $[N_u]$, $[N_V]$ is the nodal displacement, nodal electric potential, the matrix of displacement shape function and the matrix of electric potential shape function, respectively.

Strain vector, $\{\varepsilon\}$ and the electric field, $\{E\}$ can be related to the displacement field and potentials by implementing Equations (6) and (7).

$$\{\varepsilon\} = [B_u]\{u\} \tag{6}$$

$$\{E\} = [B_V]\{V\} \tag{7}$$

where

$$[B_u] = \begin{bmatrix} \frac{\partial}{\partial x} & 0 & 0 & \frac{\partial}{\partial y} & 0 & \frac{\partial}{\partial z} \\ 0 & \frac{\partial}{\partial y} & 0 & \frac{\partial}{\partial x} & \frac{\partial}{\partial z} & 0 \\ 0 & 0 & \frac{\partial}{\partial z} & 0 & \frac{\partial}{\partial y} & \frac{\partial}{\partial x} \end{bmatrix}^T \tag{8}$$

$$[B_V] = \begin{bmatrix} \frac{\partial}{\partial x} & \frac{\partial}{\partial y} & \frac{\partial}{\partial z} \end{bmatrix}^T \tag{9}$$

Elastic behavior of piezoelectric material is defined by Newton's law, as in Equation (10).

$$div\{\sigma\} = \rho \frac{\partial^2\{u\}}{\partial t^2} \quad (10)$$

where ρ is the density of the piezoelectric material. On the other hand, considering that there is no free volume charge through piezoelectric material, electrical behavior of the piezoelectric material is governed by Maxwell's equation.

$$div\{D\} = 0 \quad (11)$$

Composing Equations (1) to (11), the differential equation of motion can be formed and solved by appropriate mechanical and electrical boundary conditions, such as displacement and electrical potential or charge, respectively. However, Hamilton's variational principle, as given in Equation (12), can be extended to electromechanical couplings.

$$\delta \int_{t_1}^{t_2} (L + W)\, dt = 0 \quad (12)$$

where δ represents the first-order variation, t_1 and t_2 are the time interval. *L*, Lagrangian term is defined by the energies stored in the piezoelectric material whereas *W i*s the virtual work of the mechanical forces exerted on the system.

Using the Hamilton's variational principle and the finite element discretization, the coupled electromechanical equation of motion in matrix notation can be determined as in Equation (13).

$$\begin{bmatrix} [M] & 0 \\ 0 & 0 \end{bmatrix} \begin{bmatrix} \ddot{u} \\ \ddot{V} \end{bmatrix} + \begin{bmatrix} [C] & 0 \\ 0 & 0 \end{bmatrix} \begin{bmatrix} \dot{u} \\ \dot{V} \end{bmatrix} + \begin{bmatrix} [K_{uu}] & [K_{uV}] \\ [K_{Vu}] & [K_{VV}] \end{bmatrix} \begin{bmatrix} u \\ V \end{bmatrix} = \begin{bmatrix} \{F\} \\ \{Q\} \end{bmatrix} \quad (13)$$

where $\{F\}$ is the exciting force and $\{Q\}$ is the electrical charge vector. Here $[M]$, $[C]$, $[K_{uu}]$, $[K_{VV}]$, $[K_{uV}]$ is the mass matrix, damping matrix, structural stiffness matrix, dielectric conductivity matrix and piezoelectric coupling matrix, respectively and can be defined as Equation (14-20).

$$[M] = \sum_i [L_{ui}]^T \left[M^{(i)}\right] [L_{ui}] \quad (14)$$

$$[K_{uu}] = \sum_i [L_{ui}]^T \left[{K_{uu}}^{(i)}\right] [L_{ui}] \quad (15)$$

$$[K_{uV}] = \sum_i [L_{ui}]^T \left[{K_{uV}}^{(i)}\right] [L_{Vi}] \quad (16)$$

$$[K_{Vu}] = \sum_i [L_{Vi}]^T \left[{K_{Vu}}^{(i)}\right] [L_{ui}] \quad (17)$$

$$[K_{VV}] = \sum_i [L_{Vi}]^T \left[{K_{VV}}^{(i)}\right] [L_{Vi}] \quad (18)$$

$$\{F\} = \sum_i [L_{ui}]^T [f_i] \quad (19)$$

$$\{Q\} = \sum_i [L_{Vi}]^T [q_i] \quad (20)$$

3. AFRP Beam Case Study

3.1. Experimental set-up and validation

In accordance with the statements of electromechanical theory, an AFRP beam coupled with an embedded PZT patch was created in order to validate the electromechanical coupling. Beam was clamped at the side of the embedded PZT patch to constitute a cantilever set-up. The setup is shown in Figure 1(a), and the corresponding material and physical properties of AFRP beam and PZT patch (PI Dura-act 876.A12) are presented in Table 1.

PZT patch is considered as anisotropic whereas the AFRP material is taken as isotropic. Thus, elastic, piezoelectric and dielectric constants of PZT, which are defined in Equations (1) and (2), are tabulated in Table 2.

Using the converse effect of the piezoelectric material, the structure is excited by the piezoelectric patch and the frequency responses are measured at the tip of the beam by the Laser Doppler Vibrometer (LDV), as shown in Figure 1(b).

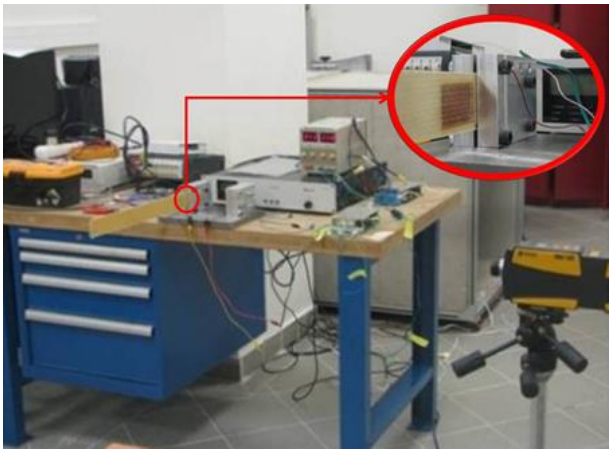

(a)

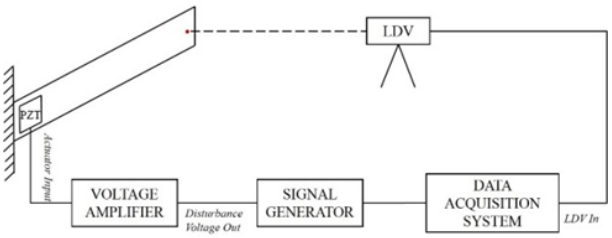

(b)

Fig. 1. (a) Cantilever beam set-up (b) Measurement system

Table 1. Mechanical properties of set-up

Property	AFRP Beam	PZT Patch
Length (mm)	500	65
Width (mm)	50	31
Thickness (mm)	1	0.5
Elastic Modulus (GPa)	73.2	-
Poisson's Ratio	0.36	0.36
Damping Ratio	0.0176	-
Density (kg/m^3)	1250	7800
Relative Permittivity, $\varepsilon_{33}^T/\varepsilon_0$	-	1750
$\varepsilon_{11}^T/\varepsilon_0$		1650
Piezoelectric Voltage Coefficient, g_{31}, (10^{-3} Vm/N)	-	-11.3

A finite element model of the experimental setup was created using the specified mechanical and electromechanical inputs. To verify the numerical model, the frequency response of the tip is calculated and compared with the experimental one. The numerical model and the comparison of the frequency responses are shown in Figure 2 and 3, respectively.

Table 2. Electromechanical properties of PZT patch

Elastic (GPa)		Piezoelectric (C/m^2)		Dielectric (10^{-12} C/Vm)	
C_{11}	123	e_{15}	11.91	ε_{11}	1649
C_{12}	76.7	e_{24}	11.91	ε_{22}	1649
C_{13}	70.25	e_{31}	-7.07	ε_{33}	1750
C_{22}	97.11	e_{32}	-7.07	-	-
C_{33}	97.11	e_{33}	13.81	-	-
C_{44}	22.26	-	-	-	-
C_{55}	22.26	-	-	-	-
C_{66}	23.15	-	-	-	-

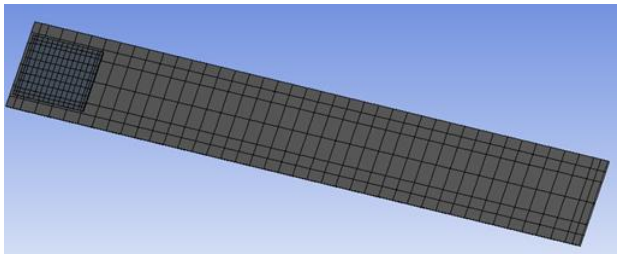

Fig. 2. FE Model of AFRP Beam

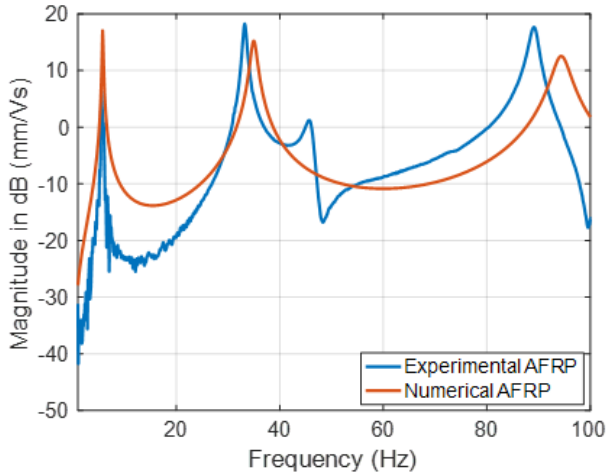

Fig. 3. Frequency response at tip of AFRP beam

As shown in Figure 3, the numerical frequency response catches the dynamic character of the experimentally measured one. It can be determined that there is a "bump" around 46 Hz of the experimental frequency response. Since the bump is a result of the effect of the constraint and has no significant meaning, this effect is not included in the numerical model. As a consequence, the numerical model of electromechanical model composed of AFRP beam and PZT patch is valid and the piezoelectric and composite material characteristics are quite correctly defined to be used for energy harvesting studies.

3.2. Energy harvesting study

In this part of the study, the energy harvesting capability of PZT patch was investigated. PZT patch is directly connected to a load resistance, R_L in order to obtain the electrical power. Using the expression of voltage across the resistive load, the output power generated by PZT patch can be calculated by employing.

$$P(\omega) = \frac{V^2(\omega)}{R_L} \quad (21)$$

Electrical circuit of PZT patch can be represented by a voltage source, V in parallel with internal capacitance C_p and internal resistance, R_p. Thus, the equivalent circuit model of the piezoelectric energy harvester with the resistive load is illustrated in Figure 4.

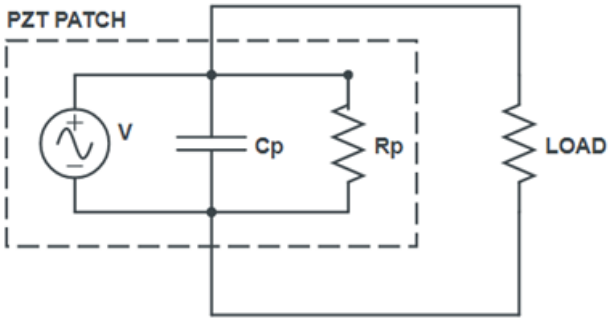

Fig. 4. Equivalent circuit model

A unit force was applied at the tip of the beam and due to the direct effect of the piezoelectric material, electrical potentials were obtained based on the different values of resistors (from 100 Ω to 50 kΩ), as shown in Figure 5. It can be seen that generated output voltages increase with increasing resistive load values and maximum output voltages are generated at resonance frequencies. Output voltage exhibits an increasing trend with the increase of the resistance value and after a certain value of resistive load, which is about 10 kΩ, the generated voltage remains almost constant. In this condition, it can be stated that the open circuit is achieved and with a resistive load of 50 kΩ, a maximum voltage of 2.68 V is generated at 19.5 Hz, second resonance frequency of the beam.

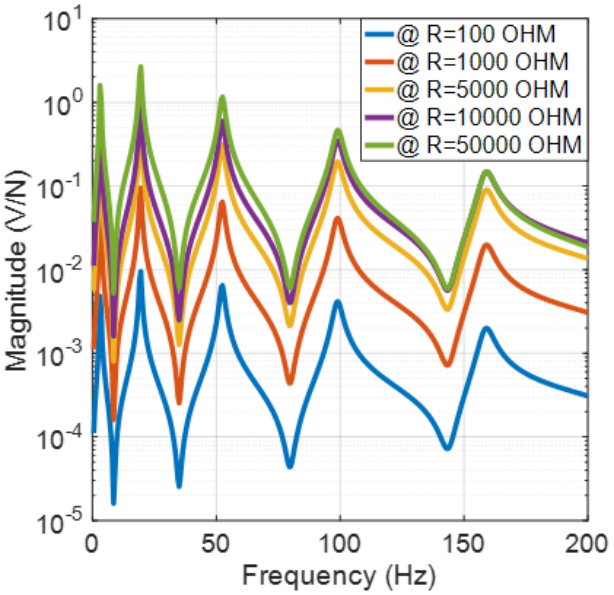

Fig. 5. Voltage outputs at various resistances

Output power was calculated by using Equation (21) and presented with respect to the resistive loads in Figure 6. As shown in the figure, maximum power was also obtained when connected to a 50 kΩ resistive load at 19.5 Hz with the value of 0.14 mW. However, it can be seen that same amount of voltage output can be achieved with the use of a resistive load of 50 kΩ and after the open-circuit condition, at higher frequencies the generated powers with respect to resistive loads become close to each other. Besides, the generated power can become lower with increasing the resistive load.

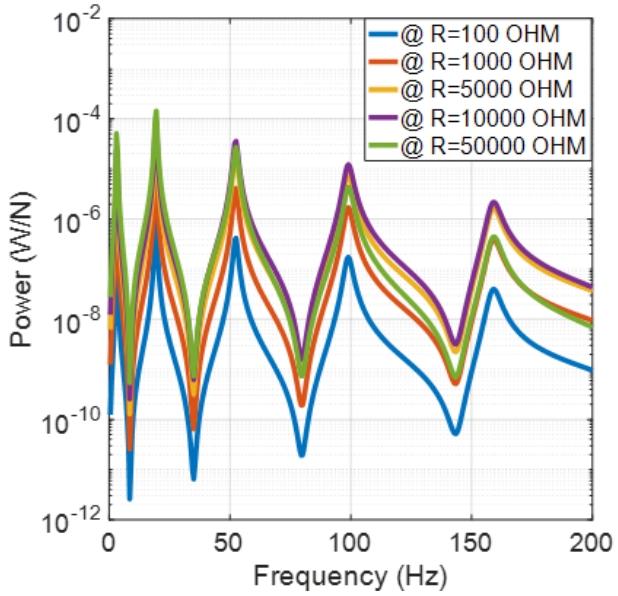

Fig. 6. Power outputs at various resistances

4. Conclusion

In this study, electromechanical modeling of piezoelectric energy harvesting by means of the finite element methods was presented and a case study composed of a cantilever AFRP beam with the embedded PZT patch was conducted.

Modal behavior of the structure is leading for piezoelectric energy harvesting. It can be stated that maximum electrical outputs are obtained at resonance frequencies of the structure. Besides, the location of the PZT patch is also critical. PZT patches should be placed at the locations where considerable strain occurs. Thus, especially for complex structures numerical analysis should be performed in order to select the appropriate locations for PZT patches.

Selecting resistive load to be connected to the PZT patch is important in terms of electrical outputs. Output voltage increases with increasing resistive loads. In the case of power generation, maximum output power differs with respect to resistive load values and there exists an optimum value of resistive load at which the maximum power can be obtained. Consequently, it is critical to model electromechanical coupling properly. Therefore, numerical study with the electromechanical modeling provides a much more cost-effective and faster solution to determine energy harvesting capabilities.

Acknowledgment

The experimental setup was developed, and the experiments were carried out during author's academic study at Koc University. The author gratefully acknowledges the in-kind support from Professor İpek Başdoğan (Koc University) for the experiment setup and Yonca-Onuk Shipyard JV for composite structures.

Conflict of interest

The author declares that he has no conflict of interest.

References

[1] M. K. Stojčev, M. R. Kosanović, L. R. Golubović, "Power management and energy harvesting techniques for wireless sensor nodes." *9th Int. Conf. on Telecommunication in Modern Satellite, Cable, and Broadcasting Services (IEEE)*, 2009. https://doi.org/10.1109/TELSKS.2009.5339410

[2] M. Safaei, H. A. Sodano, and S. R. Anton, "A review of energy harvesting using piezoelectric materials: state-of-the-art a decade later (2008–2018)," *Smart Mater. Struct.* 28, pp. 62, 2019.

[3] L. Bruant, G. Coffignal, F. Lene, and M. Verge, "Active control of beam structures with piezoelectric actuators and sensors: modeling and simulation," *Smart Materials and Structures*, 2001, vol. 10, pp. 404-408.

[4] Y. Shen and A. Homaifar, "Vibration Control of Flexible Structures with PZT Sensors and Actuators," *Journal of Vibration and Control*, vol. 7, pp. 417-451, 2001.

[5] A. Erturk and D. J. Inman, "A Distributed Parameter Electromechanical Model for Cantilevered Piezoelectric Energy Harvesters," *Journal of Vibration and Acoustics*, 2008, vol. 130, pp. 041002-15.

[6] M. I. Friswell and S. Adhikari, "Sensor shape design for piezoelectric cantilever beams to harvest vibration energy," Journal of Applied Physics, 2010, vol. 108, pp. 014901-6.

[7] Y. Aoki, P. Gardonio, M. Gavagni, C. Galassi, and S. J. Elliott, "Parametric Study of a Piezoceramic Patch Actuator for Proportional Velocity Feedback Control Loop," *Journal of Vibration and Acoustics*, 2010, vol. 132.

[8] Y. Aoki, P. Gardonio, and S. J. Elliott, "Rectangular plate with velocity feedback loops using triangularly shaped piezoceramic actuators: Experimental control

performance," *Journal of the Acoustical Society of America*, 2008, vol. 123, pp. 1421-1426.

[9] Y. Aoki, P. Gardonio, and S. J. Elliott, "Modelling of a piezoceramic patch actuator for velocity feedback control," *Smart Materials and Structures*, 2008, vol. 17, p. 015052.

[10] Z. Zyszkowski, *Podstawy Elektroakustyki; WNT*: Warszawa, Poland, 1984.

[11] J. G. Smits, S. I. Dalke, and T. K. Cooney, "The constituent equations of piezoelectric bimorph." *Sens. Actuators A Phys*. 1991, 28, 41–61.

[12] X. J. Dong, and G. Meng, "Dynamic analysis of structures with piezoelectric actuators based on thermal analogy method." *Int. J. Adv. Manuf. Technol.* 2006, 27, 841–844.

[13] H. Allik and T. J. R. Hughes, "Finite element method for piezoelectric vibration," *International Journal for Numerical Methods in Engineering*, 1970, vol. 2, no. 2, pp. 151–157.

[14] A. Benjeddou, "Advances in piezoelectric finite element modeling of adaptive structural elements: a survey," *Computers and Structures*, 2000, vol. 76, no. 1, pp. 347–363.

[15] V. Nguyen, P. Kumar, and J.Y.C. Leong, "Finite Element Modelling and Simulations of Piezoelectric Actuators Responses with Uncertainty Quantification", *Computation*, 2018, 6, no. 4: 60.

[16] E. Carrera, S. Valvano, and G. M. Kulikov, "Electro-mechanical analysis of composite and sandwich multilayered structures by shell elements with node-dependent kinematics." *Int. J. Smart Nano Mater.* 2018, 9, 1–33.

[17] S. Avdiaj, J. Setina, and N.Syla, "Modeling of the piezoelectric effect using the Finite Element Method", *Materials and Technology* 43, 2009, 6, pp. 283-291.

[18] F. Qian, Y. Liao, L. Zuo, P. Jones, "System-level finite element analysis of piezoelectric energy harvesters with rectified interface circuits and experimental validation.", *Mechanical Systems and Signal Processing*, 2021, 151, 107440.

[19] Y. Kuang, Z. J. Chew, M. Zhu, "Strongly coupled piezoelectric energy harvesters: Finite element modelling and experimental validation", *Energy Conversion and Management*, 2020, 213, 112855.

[20] R. C. Dash, D. K. Maiti and B. N. Singh, "A finite element model to analyze the dynamic characteristics of galloping based piezoelectric energy harvester", *Mechanics of Advanced Materials and Structures*, 2021. DOI: 10.1080/15376494.2021.1921316

[21] Y. Song, "Finite-element implementation of piezoelectric energy harvesting system from vibrations of railway bridge", *Journal of Energy Engineering*, 2019, vol.145

[22] A. Roy Chowdhury, N. Saurabh R. Kiran, S. Patel, "Effect of porous auxetic structures on low-frequency piezoelectric energy harvesting systems: a finite element study.", *Appl. Phys. A* 2022, 128, 62. https://doi.org/10.1007/s00339-021-05199-w

[23] IEEE Standard on Piezoelectricity ANSI/IEEE Std 176-1987, ed, 1988.